Corrosion Science 207 (2022) 110589

Contents lists available at ScienceDirect

Corrosion Science

journal homepage: www.elsevier.com/locate/corsci

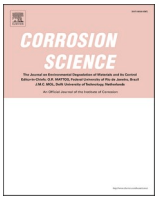

Adsorption of the prototypical organic corrosion inhibitor benzotriazole on the Cu(100) surface

Marco Turano [a], Marc Walker [a], Federico Grillo [b], Chiara Gattinoni [c,d], Gregory Hunt [e], Paul Kirkman [e], Neville V. Richardson [b], Christopher J. Baddeley [b], Giovanni Costantini [a,f,*]

[a] Department of Chemistry, University of Warwick, Coventry CV4 7AL, UK
[b] EaStCHEM-School of Chemistry, University of St. Andrews, St. Andrews KY16 9ST, UK
[c] Department of Materials, ETH Zurich, CH-8093 Zürich, Switzerland
[d] Department of Chemical and Energy Engineering, London South Bank University, London SE1 0AA, UK
[e] Strategic Research, Lubrizol Limited, Nether Lane, Hazelwood DE56 4AN, UK
[f] School of Chemistry, University of Birmingham, Birmingham B15 2TT, UK

ARTICLE INFO

Keywords:
Corrosion inhibitors
Copper
STM
XPS
HREELS
DFT

ABSTRACT

The interaction of benzotriazole (BTAH) with Cu(100) has been studied as a function of BTAH exposure in a joint experimental and theoretical effort. Scanning tunnelling microscopy (STM), X-ray photoelectron spectroscopy (XPS), high resolution electron energy loss spectroscopy (HREELS) and density functional theory (DFT) calculations have been combined to elucidate the structural and chemical characteristics of this system. BTAH is found to deprotonate upon adsorption on the copper surface and to adopt an orientation that depends on the molecular coverage. Benzotriazolate (BTA) species initially lie with their planes parallel to the substrate but, at a higher molecular coverage, a transition occurs to an upright adsorption geometry. Upon increasing the BTAH exposure, different phases of vertically aligned BTAs are observed with increasing molecular densities until a final, self-limiting monolayer is developed. Both theory and experiment agree in identifying CuBTA and $Cu(BTA)_2$ metal-organic complexes as the fundamental building blocks of this monolayer. This work shows several similarities with the results of previous studies on the interaction of benzotriazole with other low Miller index copper surfaces, thereby ideally completing and concluding them. The overall emerging picture constitutes an important starting point for understanding the mechanism for protection of copper from corrosion.

1. Introduction

The study of organic corrosion inhibitors has attracted significant interest due to their great versatility and extensive use, especially in industrial applications. In particular, benzotriazole (BTAH) has been employed for a long time mainly as a corrosion inhibitor for copper [1]. However, despite its wide and frequent usage, there is still a lack of fundamental, molecular-scale knowledge of its adsorption and orientation on copper surfaces,[2] as well as of the nature of the bonding established with the substrate [3–6]. Indeed, understanding the adsorption of BTAH on copper is non-trivial since the molecule can adsorb in a variety of forms depending on the copper surface orientation and the corrosive medium [7]. It has been shown that BTAH is able to form strong and densely packed self-assembled monolayers [8] which constitute highly effective 2-dimensional [9–11] and 3-dimensional barriers [11] against the corrosion of copper and of its alloys. However, the structural and chemical atomistic details of the BTAH-copper interaction – essential for understanding, modifying and improving the anti-corrosion properties of BTAH – have been debated for a long time in the literature and are still not fully understood [6]. While an overall picture is starting to emerge relating the efficiency of BTAH in protecting copper to its ability to chemisorb by forming strong Cu(I)–BTA complexes [12], various studies in the literature have presented different and not always fully consistent results concerning the adsorption and orientation of BTAH onto Cu surfaces [5,6,13–16].

In this regard, the study of model systems starting from the simplest, idealised cases and gradually moving onto more complex and realistic scenarios is highly beneficial to achieve a better understanding, strongly rooted in reliable experimental and theoretical evidence. Consequently, there have been a few recent studies investigating the interaction of

* Corresponding author at: Department of Chemistry, University of Warwick, Coventry CV4 7AL, UK.
E-mail address: g.costantini@bham.ac.uk (G. Costantini).

https://doi.org/10.1016/j.corsci.2022.110589
Received 13 July 2022; Received in revised form 1 August 2022; Accepted 10 August 2022
Available online 12 August 2022

BTAH with atomically flat and clean low Miller index copper surfaces under ultrahigh vacuum (UHV) conditions. These were aimed at developing a fundamental and solid understanding to be used as a series of 'knowledge building blocks' for the analysis of more complex cases such as, e.g., the interaction with real-world, polycrystalline and oxidised copper samples or the effect of BTAH on liquid-environment corrosion of copper. In particular, we contributed to some of the more detailed and comprehensive of these studies, which thus far were focussed on Cu(111) [2,9,10,16,17] and Cu(110) [11,18–20]. A common result emerging from these reports is that BTAH deprotonates upon interaction with the copper substrates at room temperature, forming a dense monolayer of strongly bound benzotriazolate (BTA) species. While a transition from essentially flat to essentially upright molecules is observed on Cu(110) with increasing molecular coverage [11], on Cu(111) BTA always adopts an upright adsorption geometry. The upright, covalently bound, high-coverage monolayer is substantially self-limiting, with further BTAH exposure resulting in second-layer, still protonated and loosely bound molecules. In this phase, the BTA radicals can form a variety of different complex structures [2,9–11,16,17] but these are all characterised by combinations of $Cu(BTA)_2$ and CuBTA metal-organic complexes. So far, only a single near edge X-ray absorption fine structure (NEXAFS) spectroscopy study has analysed the BTAH/Cu(100) system, finding that, also here, molecules are in the fully deprotonated state and form an upright standing layer upon room temperature deposition [15]. A similar methodology has also been recently applied to the fundamental study of the interaction of a sulphurated derivative of BTAH, 2-mercaptobenzothiazole (2-MBT), with copper surfaces [21–24].

Here, we intend to complete the detailed analysis of the interaction of BTAH with low Miller index copper surfaces under extremely controlled conditions, by investigating the BTAH/Cu(100) system via a combined experimental and theoretical study aimed at precisely elucidating its structural and chemical properties.

2. Materials and methods

Experiments were performed in three different UHV chambers. The preparation of the Cu(100) single crystal surfaces was very similar for all three UHV systems, with a series of Ar^+ ion sputtering cycles followed by annealing. Also, the BTAH deposition was performed in a very similar manner across the three setups by filling the deposition chamber with BTAH vapour at a certain pressure and exposing the copper surfaces to this atmosphere for a given amount of time (for more details, see supplementary material, SM). However, it should be noted that the actual values of BTAH exposure, nominally expressed in langmuir (L), could vary from one UHV chamber to another one due to potential differences in the pressure reading (position of the pressure gauges and calibration).

Scanning tunnelling microscopy (STM) experiments were performed using a variable temperature STM setup operated in constant current mode. Samples were often cooled to −140 °C for imaging, in order to decrease the surface diffusion of the adsorbed species. Analysis of the STM data was carried out by using the WSxM software [25]. X-ray photoelectron spectroscopy (XPS) measurements were carried out in the second UHV system using a monochromatic Al Kα X-ray source with energy of 1486.7 eV. The CasaXPS software [26] was used to analyse XPS data using the fitting procedure described in the SM. High-resolution electron energy loss spectroscopy (HREELS) measurements were carried out in a third UHV system. The spectrometer was operated at room temperature, in the specular geometry ($\theta_i = \theta_f = 45°$), with a nominal primary beam energy of 5 eV and a typical elastic peak resolution of ca. 50 cm^{-1} (6.2 meV full width at half maximum, FWHM). Spectra were normalised to the intensity of the elastic peak. More detailed information on the sample preparation and analysis can be found in [11].

Density functional theory (DFT) calculations of BTAH and BTA adsorbed on Cu(100) were performed with the VASP [27–29] code with the optB86b-vdW functional [30] and the projector augmented wave method [31]. The kinetic energy cut-off on the planewave basis set was 400 eV. The Monkhorst-Pack *k*-mesh used for the bulk copper unit cell was 13 × 13 × 13 *k*-points and the optimisation was run until the forces on the ions were lower than 5×10^{-4} eV/Å. With these parameters the lattice constant of copper is obtained as $a_{DFT} = 3.606$ Å, matching very well the experimentally reported value $a_{exp} = 3.61$ Å [32]. We also obtained very good agreement between calculated and experimental bond lengths for BTAH [11]. Four-layer-thick Cu(100) slabs were used, with a range of surface unit cells, having surface areas varying from 2 × 2 to 4 × 8 with respect to the Cu(100) (1 × 1) unit cell. The Monkhorst-Pack *k*-point meshes for such systems vary from (4,4,1) to (2,1,1). In all unit cells ca. 20 Å of vacuum were placed between the copper slabs in the surface normal direction and the ionic coordinates of the bottom copper layer were kept fixed at bulk values. Convergence of all the settings was thoroughly checked. The adsorption energies, E_{ads}, were calculated as:

$$E_{ads} = E_{system} - N_{BTA}E_{BTA} - E_{slab} \quad (1)$$

where E_{system} is the total energy of the whole system, consisting of N_{BTA} deprotonated BTAH molecules (i.e. BTA radicals) adsorbed on the copper slab. E_{BTA} and E_{slab} are the total energies of the BTA radical in the gas phase and of the fully relaxed Cu(100) substrate, respectively. The substrate might include N_{Cu} copper adatoms, whose formation energy, E_{Cu}^{form}, is calculated as the energy needed to extract a bulk atom onto a clean surface and amounts to 0.55 eV for Cu(100). In order to evaluate the effect of this formation energy on the adsorption of BTA on Cu(100), we consider another formulation of the adsorption energy, that we call E_{ads}^{Cu}, defined as:

$$E_{ads}^{Cu} = E_{ads} + N_{Cu}E_{Cu}^{form} \quad (2)$$

3. Results and discussion

3.1. Scanning tunnelling microscopy

3.1.1. Low coverage regime

A clean Cu(100) surface was initially exposed to 0.56 L of BTAH. Large area STM images (Fig. 1a and b) show that this results in two types of features covering the substrate and appearing bright in STM: larger ones with an irregular and often rather jagged contour and smaller and slightly dimmer ones. The latter have a lateral dimension that is compatible with the scaled molecular model of individual flat lying BTAs (Fig. 1c), an adsorption configuration that is confirmed more rigorously by DFT and HREELS (vide infra). The observation of a low molecular coverage flat (or nearly flat) phase resembles very closely what has been reported on Cu(110). However, while on Cu(110) the BTA molecules formed an ordered c(4 ×2) structure [11,18], no ordered flat-lying supramolecular structure was observed on Cu(100), irrespectively of the molecular coverage. Nevertheless, in higher resolution images (e.g. Fig. 1c) it is still possible to observe some short, locally ordered molecular rows with a minimum distance of (0.83 ± 0.08) nm, which is compatible with a × 3 periodicity of the underlying atomic copper lattice along $[01\bar{1}]$ or [011] (highlighted by a red contour in Fig. 1c). Occasionally, as can be expected from the square symmetry of the substrate, these rows combine into very small patches of a few molecules arranged into a local 3 × 3 superstructure, although these are extremely rare. The overall impression is that there must be an effective intermolecular short-range repulsion not allowing the BTA molecules to get closer than the × 3 minimum distance. This might be due to a combination of factors such as electrostatic repulsion between negatively charged azole groups and strain induced into the substrate by the molecular adsorption. The BTA molecules appear to cover the entire surface, including also the larger and brighter features. The STM-measured apparent height of these features is compatible with that

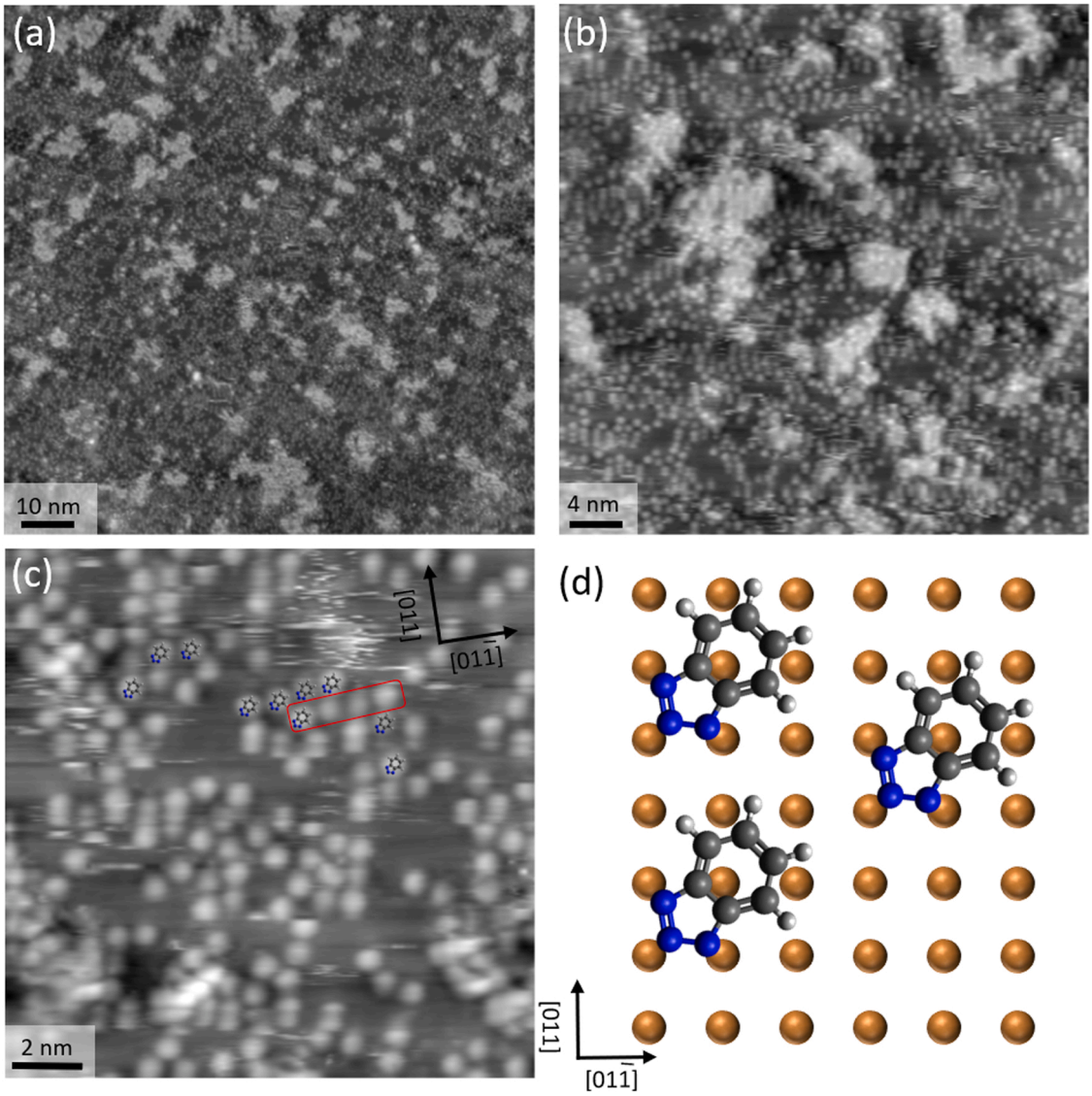

Fig. 1. Low coverage regime of BTA obtained by exposing the Cu(100) surface to 0.56 L of BTAH. (a) 100 × 100 nm^2 STM image showing some brighter Cu monoatomic island having irregular contours. (b) 40 × 40 nm^2 STM image showing Cu monoatomic island and BTA molecules. (c) 15 × 15 nm^2 STM image with scaled molecular models of BTA superimposed onto isolated bright features. The intention is to compare the lateral size, not to infer the molecular orientation. An example of local ordering of BTA molecules along [01$\bar{1}$] with × 3 periodicity is highlighted by a red contour. (d) Proposed model of BTA adsorbed on Cu(100) at low molecular coverage. Cu atoms are brown while H atoms are white, N blue and C grey. Tunnelling parameters were $I = 100$ pA, $V_{bias} = -1$ V (applied to the sample). All STM images were acquired after cooling the sample to ca. −140 °C.

of a monoatomic Cu(100) terrace (Fig. S1) and they are therefore identified as small copper monoatomic islands. The origin of their formation is unclear but they are probably a consequence of the strong interaction between the BTA molecules and copper.

3.1.2. *High molecular coverage regime*

By exposing the Cu(100) surface to 0.7 L of BTAH, a different phase was observed (dubbed high-density phase 1, HD1) which seems rather disordered and characterised by bright features of varying apparent lateral size (see Fig. S2). While it was not possible to further resolve these features, it was also quite apparent that they had a high surface density and that their size was not compatible with that of flat molecules. As a result, we tentatively assign them to (mostly) upright standing molecules. Increasing the BTAH exposure further to 3.2 L, resulted in the appearance of a new high-density molecular phase (high-density phase 2, HD2) which is ordered and that, initially, coexists with small patches of HD1 (e.g. see the top third of Fig. 2a). HD2 is characterised by extended bright rows that, in the STM images in Fig. 2, run along the substrate [011] direction and are separated by a distance of (1.49 ± 0.12) nm along [01$\bar{1}$] (compatible with a ×6 periodicity of the underlying copper atomic lattice). Clearly, due to the symmetry of the Cu(100) substrate, the same structure can be seen rotated by 90° in different regions of the surface, with the rows running along [01$\bar{1}$] (see Fig. S3). A closer inspection of higher resolution images (e.g. Fig. 2c), reveals a regular structure within these rows with a periodicity of (1.77 ± 0.16) nm which is compatible with a × 7 the periodicity of Cu(100). Additionally, between two consecutives rows one can distinguish further, more sparse features that are regularly spaced at a distance of (0.87 ± 0.09) nm, a periodicity which is not compatible with any integer multiple of the Cu(100) atomic lattice but close to the half-integer value of 3.5.

The bright features constituting the [011]-oriented rows and those in between the rows have different size, elongation and orientation and their precise appearance depends heavily on the status of the STM tip. None of them is compatible with flat-lying BTA molecules but their

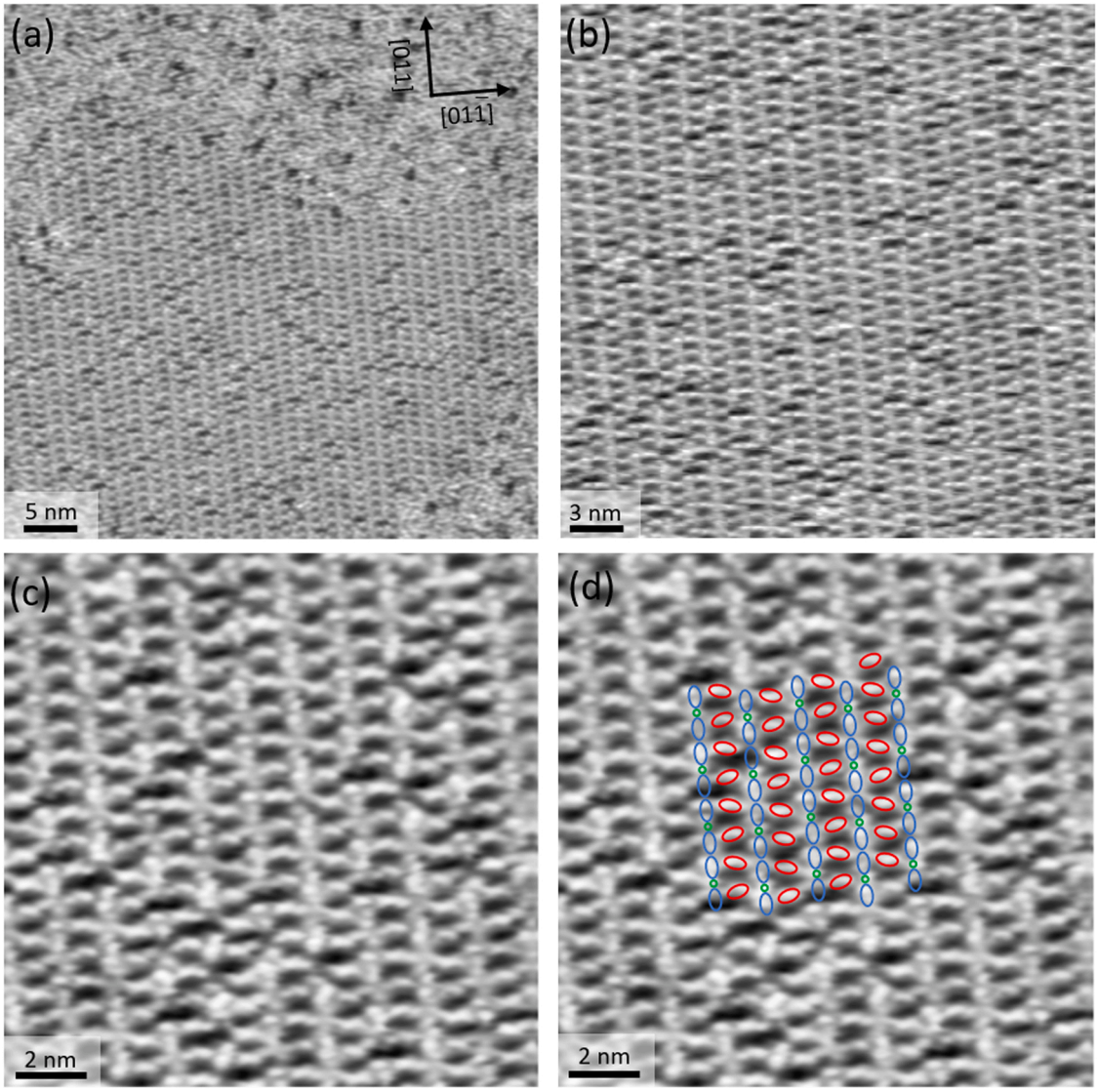

Fig. 2. High coverage regime of BTA on Cu(100), obtained by exposing the copper surface to 3.2 L of BTAH. (a) 50 × 50 nm^2 STM image showing small patches of the disordered HD1 phase (upper part) coexisting with the highly ordered HD2 phase which covers most of the sample. (b) 30 × 30 nm^2 and (c) 15 × 15 nm^2 STM image showing higher magnifications of the HD2 phase. (d) same image as (c) with superimposed schematic representation of a tentative model for HD2. Blue and red ovals represent BTA molecules and green circles Cu adatoms. Tunnelling parameters were $I = 100$ pA, $V_{bias} = -1$ V in (a), $I = 100$ pA, $V_{bias} = -1$ V in (b) and $I = 100$ pA, $V_{bias} = -1$ V in (c). All STM images were acquired after cooling the sample to ca. −140 °C.

lateral dimension is consistent with that of molecules with their plane perpendicular to the surface. The assignment to upright molecules, which is only provisional when based on the STM data, is confirmed by DFT calculations and HREELS measurements (vide infra) and indicates a transition from an almost flat to an almost upright molecular adsorption with increasing coverage, similar to what we observed for the BTA/Cu (110) system [11]. In the case of BTA/Cu(100), however, it is not possible to identify a clear-cut appearance of individual upright BTA molecules and any molecular model of the adsorption superstructure is, therefore, necessarily speculative. Fig. 2d shows a tentative assignment of the different features appearing in the STM images. The bright protrusions within the [011]-oriented rows are attributed to pairs of BTA molecules (blue ovals) coordinating a copper adatom (green circle) into $Cu(BTA)_2$ metal-organic complexes. The features between the rows are assigned to single BTA molecule, possibly bound to a copper adatom in a CuBTA complex. The latter seem to have a (mostly regular) alternating orientation, with their main axes oriented at about ± 10° with respect to [01$\bar{1}$]. This is probably caused by the separation between the CuBTA complexes along [011] not being constant but alternating between × 3 and × 4 with respect to the Cu(100) substrate; this results in an average separation of × 3.5, in agreement with the value measured by STM.

The presence of CuBTA and $Cu(BTA)_2$ complexes is compatible with the lowest energy adsorption configurations predicted by DFT calculations for upright molecules (vide infra). Moreover, both types of metal-organic complexes were reported for BTA on Cu(110) [11] and Cu(111) [10] and parallel rows of [011]-oriented $Cu(BTA)_2$ complexes with a similar internal periodicity (ca. 1.8 nm) were also found in the BTA/Cu (111) system [10]. Based on this model, the darker, randomly distributed features observed in the STM images can be interpreted as defects in the supramolecular structure caused by vacancies of individual BTA molecules. Despite this overall good agreement with the experimental and theoretical data, we reiterate that this is only a tentative model and that the existence of alternative models with an equivalent (or possibly even better) fit, cannot be excluded.

Increasing the total BTAH exposure to 4.2 L resulted in the appearance of a further molecular structure (high-density phase 3, HD3, see Fig. 3a and b) which initially coexists with HD2 and then, by increasing the total BTAH exposure to 5.0 L, takes over the entire surface. The

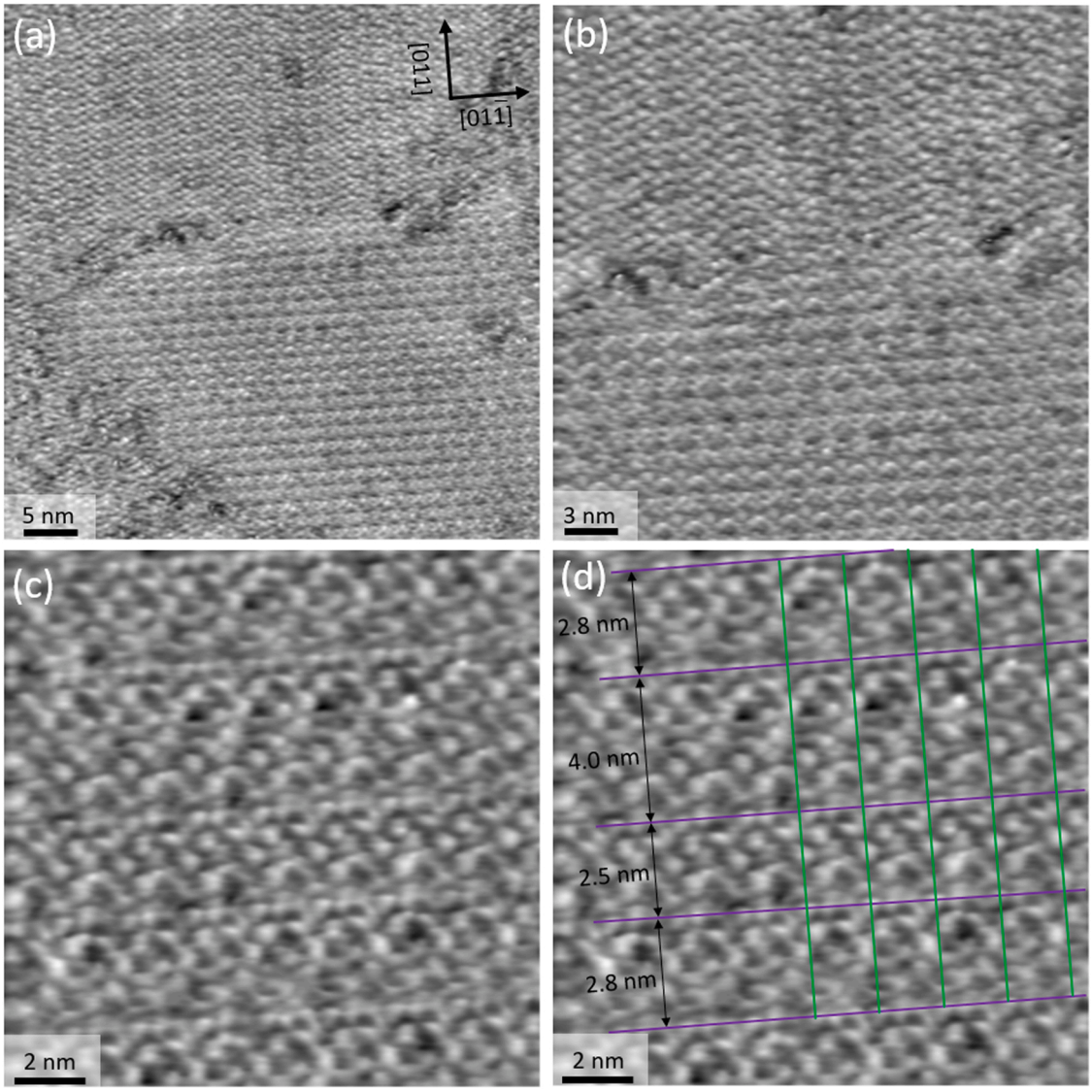

Fig. 3. Higher coverage regime (HD3) of BTA on Cu(100) obtained by exposing the copper surface to 4.2 L of BTAH. (a) 50 × 50 nm^2 image showing two ordered islands rotated by 90° with respect to each other together with small patches of non-ordered molecules (left bottom corner). (b) 30 × 30 nm^2 image showing the boundary between two 90°-rotated molecular domains (zoom of the central part of (a)). (c) 15 × 15 nm^2 image showing a magnification of the lower domain in (b). (d) same image as (c) with purple lines showing the separation between contiguous [01$\bar{1}$]- oriented stripes and green lines indicating the periodicity within the stripes. Tunnelling parameters were $I = 80$ pA, $V_{bias} = -1$ V in (a), $I = 80$ pA, $V_{bias} = -1$ V in (b) and $I = 100$ pA, $V_{bias} = -1$ V in (c). All STM images were acquired after cooling the sample to ca. −140 °C.

images acquired on HD3 were even more difficult to interpret than those on HD2 and a similar strong dependence of the image appearance on the status of the STM tip was noted. However, a constant observation was the presence of stripes that, in Fig. 3c, run along [01$\bar{1}$]. These stripes have a variable width (see e.g. Fig. 3d) with a measured average of (2.87 ± 0.17) nm. Several different bright features can be recognised within the stripes and although their appearance changes even within the same STM image (e.g. Fig. 3c), they display a common periodicity of (1.81 ± 0.15) nm along the main axis of the stripe (separation between the green lines in Fig. 3d). We note that this distance is comparable with the lateral dimension of a $Cu(BTA)_2$ complex aligned along [01$\bar{1}$], in accordance with that found by DFT (vide infra). The individual bright features have sizes that are compatible with that of upright-standing single or pairs of BTA molecules which, as for HD2, we propose to interpret as CuBTA and $Cu(BTA)_2$ metal-organic complexes locally organised into specific patterns. However, we refrain from suggesting any further detailed molecular model for HD3, as this would be excessively speculative based on the available STM data. Similarly to what we observed for HD2, due to the twofold symmetry of the Cu(100) substrate, HD3 also presents two equivalent domains rotated by 90° with respect to each other (see Fig. S4). While it is difficult to make any precise statement without a clear molecular model, the qualitative impression obtained from considering the density of individual bright features in the STM images is that HD3 is more densely packed than HD2 – as would be expected given that it appears at higher BTAH exposures. HD3 also appears to be self-limiting since no major changes were observed in the morphology of the sample by increasing the amount of BTAH up to 10 L through successive exposures. The only modification that was observed was a decrease of the width of the stripes with increasing BTAH exposure and the occasional appearance of 'fuzzy' areas in the STM images, that we interpret as an indication of loosely bound second layer molecules (Fig. S5).

3.2. Density functional theory

DFT calculations were performed on a range of systems including isolated BTA molecules, CuBTA and $Cu(BTA)_2$ metal-organic complexes and extended $(CuBTA)_n$ chains, although a stable configuration could not be found for the latter structure on the Cu(100) surface. The most energetically stable system was found to be simply an isolated BTA molecule adsorbed with a small tilt with respect to the surface. The adsorption energy for this system is $E_{ads} = -3.78$ eV/mol. Fig. 4a shows this structure, presenting a molecule with an 8° inclination with respect to the surface and bond lengths between the N atoms of the azole moiety and the surface Cu in the 2.1–2.4 Å range. The Cu(100) surface, with equally spaced Cu atoms at a distance of 2.54 Å, forms a good template for the azole moiety to bond on. An even better template is obtained when a Cu adatom is added to the surface, and one of the N atoms binds to it, allowing the formation of slightly shorter N-Cu bonds (Fig. 4b). In this case the adsorption energy, without considering the formation energy of the adatom (Eq. 1), is $E_{ads} = -4.10$ eV/mol, which however reduces to $E_{ads}^{Cu} = -3.54$ eV/mol when the adatom formation energy is included in the calculation (Eq. 2). In Fig. 4b it can be seen that the adatom in the CuBTA complex is almost in a top position with respect to the Cu substrate, while the computed most stable configuration for an isolated adatom on a clean Cu(100) surface is in a fourfold hollow position, with an adsorption energy which is almost 1 eV lower with respect to the top position. The location of the adatom in the CuBTA complex is thus strongly dependent on the position of the BTA molecule and a trade-off between stabilising BTA and adsorbing the adatom is needed. Thus, the small gain in energy due to the stronger bonding of BTA to Cu does not offset the energy required to bring the adatom onto the surface. $Cu(BTA)_2$ complexes were also modelled in two different configurations, with the N-Cu-N bonding direction aligned along [010] and [110], as shown in Fig. 4c and d, respectively. A small energy difference was found between the most stable structures in these two directions, with a preference of ~0.02 eV/mol for the [110] direction, confirming the preferential alignment observed in experiments. The adsorption energy, following Eq. 2, for the $Cu(BTA)_2$ complex is $E_{ads}^{Cu} = -3.74$ eV/mol.

Similarly to the Cu(110) [11] systems, the observed experimental structure at high coverage is composed of upright molecules, despite the flat configurations being more energetically stable (although only by a small margin), when considering the adsorption energy per molecule (Eq. 2). However, it should be noted that the adsorption footprint of a flat molecule is of ~50 $Å^2$, compared to the ~30 $Å^2$ of a molecule in an upright metal-organic complex. As such, the adsorption energies per unit area are significantly lower for upright than for the flat molecules. This consideration underpins the experimental observations (by STM, XPS and HREELS) of a transition from flat to upright adsorbed molecules by increasing the exposure to BTAH vapour.

3.3. X-ray photoelectron spectroscopy

XPS measurements were carried out by performing a number of successive molecular depositions, in which the Cu(100) surface was exposed for increasing amounts of time to a typical BTAH pressure of ca. 2×10^{-9} mbar. Together with XP survey scan spectra, higher resolution spectra for the Cu $2p_{3/2}$, N 1*s* and C 1*s* binding energy (BE) regions were acquired after each molecular deposition. The integrated intensities of these spectra are represented in Fig. 5 as a function of the BTAH exposure time (which might be different from the total molecular coverage because of the non-constant sticking coefficient). The trends of the

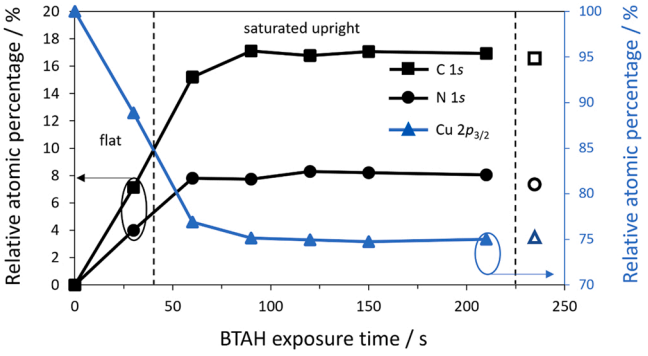

Fig. 5. Relative atomic percentages for the C 1 *s*, N 1 *s* and Cu $2p_{3/2}$ XPS signals as function of the BTAH exposure time at a pressure of ca. 2×10^{-9} mbar. Empty symbols refer to the XPS signals measured after annealing the saturated upright phase to 130 °C .

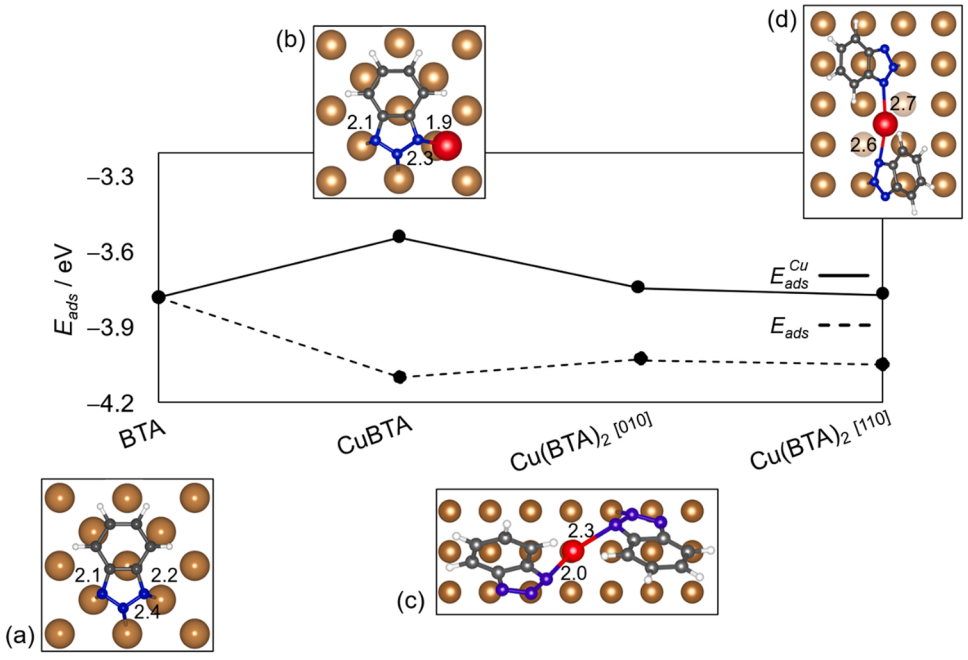

Fig. 4. Adsorption energies for the most stable adsorbed structures of BTA on Cu(100). The solid line in the graph connects the adsorption energies including the formation energy of the copper adatom, the dashed line those without. The configurations of the different structures are also shown, with Cu atoms in brown, Cu adatoms in red, N blue, C grey and H white: (a) isolated flat BTA; (b) flat CuBTA complex; (c) upright $Cu(BTA)_2$ complex aligned along [010]; (d) upright $Cu(BTA)_2$ complex aligned along [110]. The numbers correspond to the bond lengths expressed in Å.

substrate and of the molecular signals clearly show that the surface molecular coverage increases up to an exposure of ca. 90 s and then rapidly saturates with successive BTAH exposures. This is a validation of the observation anticipated by STM that the mostly upright form of BTA monolayer is self-limiting. While it is not possible to directly compare the BTAH exposures for the STM and XPS experiments (see SM), it is reasonable to assume that the saturation of the N 1*s*, C 1*s* and Cu $2p_{3/2}$ signals in Fig. 5 corresponds to the establishment of the HD3 phase determined in STM. The transition between the flat and the upright orientations of BTA in Fig. 5 is estimated based on this assumption.

3.3.1. Low coverage regime

Fig. 6a and b show the low coverage spectra in the N 1*s* and C 1*s* regions, respectively, measured after 30 s of BTAH exposure at a pressure of about 2×10^{-9} mbar. The resulting molecular phase should correspond to mostly flat-lying BTA species as identified in the STM and HREELS sections. The best fit for the N 1*s* spectrum is obtained with two components (Fig. 6a). The orange peak at lower BE (399.5 eV) is assigned to the N-C environment, while the blue peak at higher BE (400.2 eV) is assigned to the N-N environment, in good agreement with previous literature on BTA/Cu(111) [16] and BTA/Cu(110) [11]. The absence of a third peak at higher BE that is typically assigned to the H-N-C environment [11,33,34], is a confirmation that the molecules are fully deprotonated. The ratio between the integrated intensities of the two peaks is 1.8 which is not too dissimilar from the expected value of 2.0. A similar small difference was also observed for BTA/Cu(110) [11] and could be due to variations in the local binding environments of the three nitrogen atoms coordinating with the Cu substrate atoms. These variations can be responsible for chemical shifts of up to 0.8 eV [16], resulting in an effective redistribution of the relative intensities between the N-C and N-N species.

The C 1*s* spectrum was also best fitted with two components (Fig. 6b), a lower BE red peak (284.6 eV) assigned to the C-C environment and a higher BE purple peak (285.3 eV) assigned to the C-N environment, similarly to that observed for BTA&Cu/Au(111)[33,34]. The ratio between the integrated intensities of the higher and the lower BE components is larger than one, i.e. opposite to what expected from the stoichiometry of BTA. Even though the reason for this discrepancy is not fully clear, we note that a very similar scenario was also observed for BTA/Cu(110) [11].

3.3.2. High coverage regime

The XP spectra corresponding to the five points of higher BTAH exposure time in Fig. 5 are very similar. Fig. 6c and d show the N 1*s* and C 1*s* regions, respectively, measured after 210 s of BTAH exposure at a pressure of about 2×10^{-9} mbar, which is likely to produce the self-limiting upright phase HD3 discussed in the STM section. The N 1 *s* spectrum (Fig. 6c) is reproduced by two components (399.5 eV, orange, and 400.3 eV, blue) in an identical model to that used to fit the lower coverage phase and, as result, these two components are assigned to the N-C and the N-N environments, respectively. An alternative analysis of the N 1*s* signal can be obtained by including a small component at higher BE and results in a similarly good fit (Fig. S7a). This extra component could be interpreted as the signature of a small percentage of protonated second-layer molecules, which however disappears upon annealing to 130 °C (Fig. S7c). An analogous behaviour has been observed for the BTAH/Cu(110) system [11].

In this coverage regime, the C 1*s* spectrum is described by two

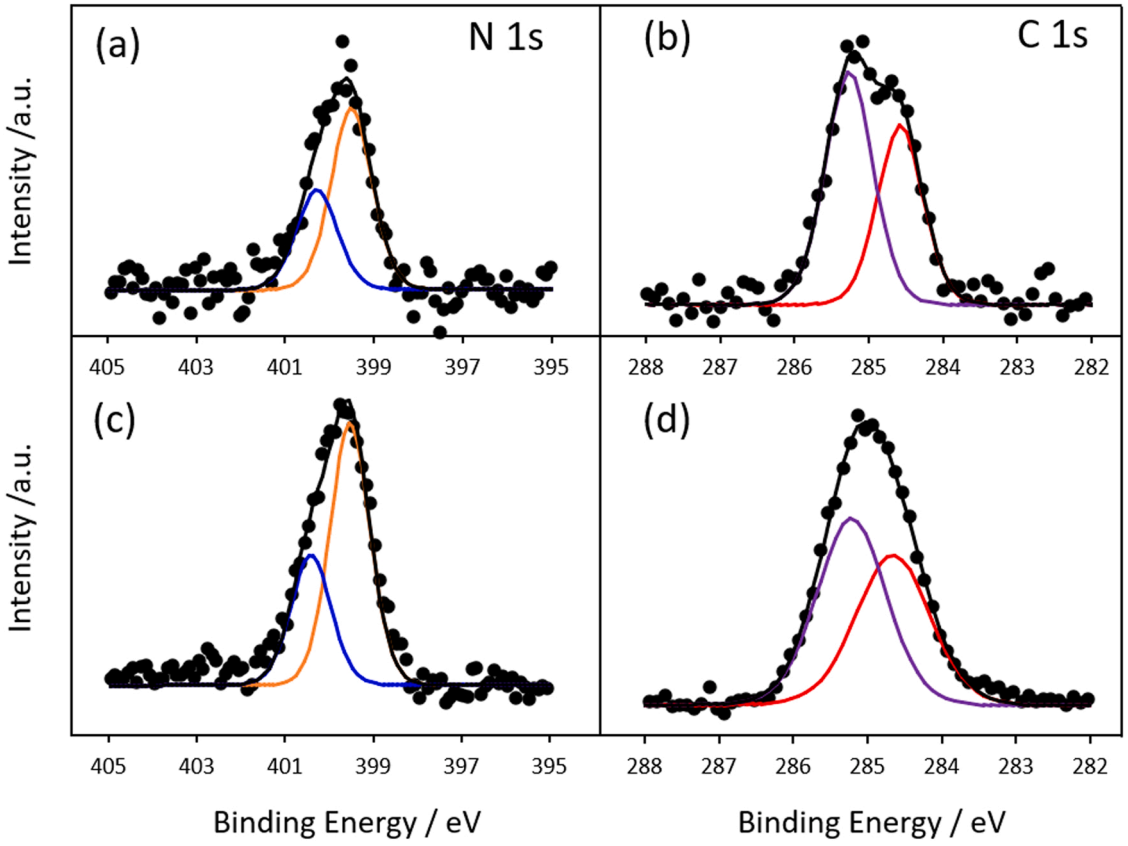

Fig. 6. XP spectra showing the N 1*s* (left column) and the C 1*s* (right column) BE regions obtained for different exposures of the Cu(100) surface to a BTAH gas pressure of about 2×10^{-9} mbar. (a) N 1 *s* spectrum after 30 s of BTAH exposure, representing the low coverage phase in which BTA molecules lie mostly flat on the surface. (b) Corresponding C 1*s* spectrum. (c) N 1*s* spectrum after 210 s of BTAH exposure, representing the HD3 phase of BTA molecules in a mostly upright configuration. (d) Corresponding C 1*s* spectrum. All data points are represented by black circles, coloured lines indicate the different fit components and the best fit curve is shown by a black line.

components (Fig. 6d). The lower BE component (read peak) is centred at 248.7 eV and thus assigned to the C-C environment. The purple peak at higher BE (285.2 eV) is shifted by 0.1 eV with respect to the corresponding peak measured at low coverage (Fig. 6b) and, as a result, is assigned to C-N environment. The shift toward lower binding energies was similarly observed also for BTAH/Au(111) [33] and BTAH/Cu(110) [11] and might be due to a change in the surface dipole layer generated by the transition of the molecular orientation, from almost parallel (low coverage) to almost perpendicular (high coverage) with respect to the substrate. Similar to the low coverage regime, the ratio between the integrated intensities of the higher and the lower BE components is larger than one, again opposite to what expected from the stoichiometry of BTA. However, an alternative fit where the relative ratio of these two components is larger than one could also be obtained, with the residual fitting error only 7% worse than for the fit shown in Fig. 6d.

3.4. High resolution electron energy loss spectroscopy

Vibrational spectra following exposure of the Cu(100) surface to increasing amounts of BTAH vapour are shown in Fig. 7. Energy losses observed experimentally, and their assignments, are summarised for ease of comparison in Table 1.

The energy loss spectrum recorded after exposing the Cu(100) surface to 0.5 L of BTAH at room temperature (Fig. 7, black spectrum), shows only a peak at around 770 cm^{-1} due to the CH out of plane (γ, oop) bend of the benzene ring, and a raised background between 1000 and 1600 cm^{-1}. Notably, the aromatic ν CH stretch, expected at about 3000 cm^{-1}, is not present. The observation of such vibrations agrees well with BTA moieties adsorbing flat with respect to the surface, as shown in STM images recorded for the low coverage regime (Fig. 1). This adsorption configuration is inferred by the presence of γ CH and absence of ν CH: in fact, if the molecular plane is parallel to the surface, the former mode is dipole active, whereas the latter is largely inactive. The state of protonation cannot be determined form this spectrum, as, similarly to ν CH, also the ν NH mode is largely dipole inactive for parallel adsorption [36].

With increasing the exposure to 1 L of BTAH (Fig. 7, green curve), a faint breathing mode of the benzene ring is seen at 675 cm^{-1}, the γ CH mode at around 770 cm^{-1} increases in intensity, a peak assigned to an out of plane bend of the aromatic ring develops at 985 cm^{-1} (over a generally increased background) and a very week signal appears at

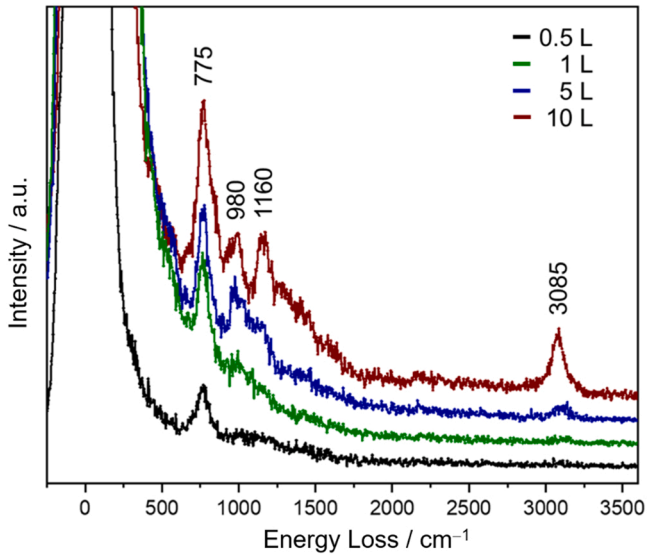

Fig. 7. HREEL spectra following exposure of Cu(100) to increasing amounts of BTAH at room temperature. Spectra are offset vertically for clarity. Exposures to BTAH are indicated in langmuir. Only the main peaks are labelled.

Table 1
Observed energy losses/cm^{-1} and assignments.

Mode	0.5 L	1 L	5 L	10 L
ν CH		3140	3135	3085
ν CC + ν CN				1615
δ NH (H-bonded)				1570
ν NNN (N… Cu(I))				1290
ν NNN + ν CH			1155	1160
γ CH		985	975	985
γ CH	770	770	765	770
C_6H_4 ring breathing		675	670	660

ν stretch, γ out of plane bend, δ in plane bend

3140 cm^{-1} (CH stretch). The observation of these vibrations indicates an increase in coverage, with an adsorption geometry in which the vast majority of the BTA species still have their molecular plane largely parallel to the surface, with potentially the presence of some molecules orientated more upright. Indeed, this spectrum can represent a packing configuration expected just prior to the formation of the HD1 phase reported in Fig. S2. It is important to stress, yet again, that the nominal exposure in langmuir may differ from one UHV chamber to another, as the shape, volumes and geometries of the different systems are different, and the ion gauges are not calibrated for BTA/BTAH.

After an exposure of 5 L (Fig. 7, blue curve), the shoulder due to the benzene ring breathing mode at 670 cm^{-1} is more evident and the CH oop bending mode of the benzene ring at 770 cm^{-1} keeps increasing in intensity. Also, the CH out of plane bend of the benzene ring at 975 cm^{-1} increases in intensity and the stretching mode of the triazo moiety (ν NNN), coupled with a CH stretch emerges from the background at 1155 cm^{-1}. The ν CH mode at 3135 cm^{-1} increases in intensity and broadens. The observation of ν NNN, along with the increase in intensity of ν CH, is a clear indication that the transition to an adsorption geometry in which the molecular plane is more upright is occurring. This is in agreement with the STM observations of the formation of a denser layer with increased exposure to BTAH, which requires BTA species to transition to a more upright geometry, similarly to what observed for the adsorption of BTAH on Cu(110) [11].

The spectrum recorded after 10 L exposure (Fig. 7, brown curve), shows a dramatic increase of all energy loss signals. In particular, the ν CH mode, which shifts to 3085 cm^{-1}, increases proportionally much faster than γ CH at 775 cm^{-1}. The variation of the γ CH: ν CH ratio indicates that the transition to an almost fully upright phase has occurred, which is in full agreement with the STM measurements. As a further confirmation, also ν NNN (1160 cm^{-1}) shows a substantial intensity increase. Additional vibrations can now be recorded at 1290 cm^{-1}, assigned to stretches of the triazole group in an N…Cu(I) environment [9–11,33,34,36], at 1310 cm^{-1}, assigned to a γ CH coupled with a breathing mode of the benzene ring, and 1615 cm^{-1}, attributed to a combination of ν CC + ν CN. The mode at 1570 cm^{-1} is assigned to an in-plane bend of the NH group for hydrogen bonded NH; this is accompanied by a change in the profile of the 980 cm^{-1} mode, which now shows a combination of γ NH and γ CH [11,33–35]. This indicates that, other than a fully upright phase, some other flat lying molecules are adsorbed on the surface and agrees with the occasional observation of 'fuzzy' areas in the STM images, thought to be related to loosely bound second layer BTAH molecules (Fig. S5).

A further confirmation of the self-limiting nature of the HD3 phase ad-layer is obtained via vibrational spectroscopy too, as shown in Fig. S8: in fact, spectra obtained after exposing to 10 L and 20 L of BTAH vapours are essentially superposable. This is also consistent with the trends of the XP signals in the "saturated upright" regime of Fig. 5.

4. Conclusions

In this work the interaction of BTAH with the Cu(100) surface has been studied both experimentally, under UHV conditions by means of

STM, XPS and HREELS, and theoretically, by means of DFT. In particular, our study has analysed the structural and chemical properties of this prototypical organic corrosion inhibitor when adsorbed at different molecular coverages on the (100) orientation of copper. Our results demonstrate that benzotriazole readily deprotonates to its benzotriazolate form upon room temperature deposition. With increasing BTAH exposure, the molecular orientation changes from being mostly parallel to the substrate to being mostly perpendicular to it. This transition is rationalised by the theoretical finding that, on Cu(100), flat BTAs have a higher adsorption energy per molecule, while upright BTAs have a higher adsorption energy per unit area. The molecular packing is shown to increase also for the vertical BTAs, with transitions to successively denser phases being observed upon incrementing the BTAH exposure until a final, self-limiting monolayer of upright molecules is formed. While a precise molecular-scale identification of its structure was not possible, the combination of STM, XPS, HREELS and DFT clearly demonstrated that CuBTA and $Cu(BTA)_2$ metal-organic complexes are the fundamental building blocks for this monolayer.

When comparing these results with those reported for BTAH/Cu(111) and BTAH/Cu(110), an overall picture emerges with several common characteristics, such as the formation of a self-limiting, dense organic overlayer where upright adsorbed deprotonated molecules are strongly bound with copper adatoms into metal-organic complexes. The present work thus ideally completes and concludes previous studies of the interaction of benzotriazole with low Miller index copper surfaces, constituting the starting point for future studies focussed on elucidating the molecular scale mechanism by which BTAH acts as an anticorrosion agent for copper.

Data statement

All data needed to evaluate the conclusions in the paper are present in the paper and/or the Electronic Supplementary Material. Additional data related to this paper may be requested from the authors.

CRediT authorship contribution statement

M.T. performed and analysed the STM measurements, analysed the XPS data and wrote a first draft of the manuscript. M.W. performed the XPS measurements and participated in their analysis. F.G. helped in devising the experimental plan, performed and analysed the HREELS measurements and wrote the corresponding part of the paper. C.G. performed and analysed the DFT calculations and wrote the corresponding part of the paper. G.H. and P.K. proposed the scientific problem and contributed to the conception of the project. N.V.R. and C.J.B. discussed the analysis of HREELS data. G.C. conceived and coordinated the research project and wrote most of the paper. All authors participated in discussing the data and editing the manuscript.

Declaration of Competing Interest

The authors declare that they have no known competing financial interests or personal relationships that could have appeared to influence the work reported in this paper.

Data availability

Data will be made available by the corresponding author on reasonable request. The HREELS data supporting this publication can be accessed at https://doi.org/10.17630/93ee08b5-7ebd-4c3a-9a5b-b191d1839a4b

Acknowledgments

M.T. gratefully acknowledges financial support from Lubrizol Limited and thanks the Engineering and Physical Sciences Research Council (EPSRC) grant EP/L015307/1 for the Molecular Analytical Science Centre for Doctoral Training (MAS-CDT). C.G. acknowledges the use of the Euler cluster at ETH Zurich for the DFT calculations. F.G. acknowledges funding from the EPSRC (grant EP/S027270/1).

Appendix A. Supporting information

Supplementary data associated with this article can be found in the online version at doi:10.1016/j.corsci.2022.110589.

References

[1] Procter and Gamble Ltd, Compositions for Inhibiting Metal Tarnish, British Patent, 1947.
[2] F. Li, Z. Wang, Y. Jiang, S. Sun, S. Chen, S. Hu, C. Li, DFT study on the adsorption of deprotonated benzotriazole on the defective copper surfaces, Corros. Sci. (2021), 109458.
[3] A. Kokalj, S. Peljhan, Density functional theory study of ATA, BTAH, and BTAOH as copper corrosion inhibitors: adsorption onto Cu (111) from gas phase, Langmuir 26 (2010) 14582–14593.
[4] A. Kokalj, S. Peljhan, M. Finsgar, I. Milosev, What determines the inhibition effectiveness of ATA, BTAH, and BTAOH corrosion inhibitors on copper? J. Am. Chem. Soc. 132 (2010) 16657–16668.
[5] S. Peljhan, A. Kokalj, DFT study of gas-phase adsorption of benzotriazole on Cu (111), Cu (100), Cu (110), and low coordinated defects thereon, Phys. Chem. Chem. Phys. 13 (2011) 20408–20417.
[6] M. Finšgar, I. Milošev, Inhibition of copper corrosion by 1, 2, 3-benzotriazole: a review, Corros. Sci. 52 (2010) 2737–2749.
[7] Y.I. Kuznetsov, Triazoles as a class of multifunctional corrosion inhibitors. A review. Part I. 1, 2, 3-Benzotriazole and its derivatives. Copper, zinc and their alloys, Int. J. Corros. 7 (2018) 271–307.
[8] C.D.A. Inc., Benzotriazole: an effective corrosion inhibitor for copper alloys, Copper Development Association, https://www.copper.org/publications/pub_list/pdf/a1349.pdf, 2021 (accessed 19 May 2022).
[9] F. Grillo, D.W. Tee, S.M. Francis, H. Früchtl, N.V. Richardson, Initial stages of benzotriazole adsorption on the Cu (111) surface, Nanoscale 5 (2013) 5269–5273.
[10] F. Grillo, D.W. Tee, S.M. Francis, H.A. Früchtl, N.V. Richardson, Passivation of copper: benzotriazole films on Cu (111), J. Phys. Chem. C 118 (2014) 8667–8675.
[11] M. Turano, M. Walker, F. Grillo, C. Gattinoni, J. Edmondson, O. Adesida, G. Hunt, P.M. Kirkman, N.V. Richardson, C.J. Baddeley, Understanding the interaction of organic corrosion inhibitors with copper at the molecular scale: benzotriazole on Cu (110), Appl. Surf. Sci. 570 (2021), 151206.
[12] I. Dugdale, J. Cotton, An electrochemical investigation on the prevention of staining of copper by benzotriazole, Corros. Sci. 3 (1963) 69–74.
[13] K. Mansikkamäki, C. Johans, K. Kontturi, The effect of oxygen on the inhibition of copper corrosion with benzotriazole, J. Electrochem. Soc. 153 (2005) B22.
[14] C. Gattinoni, A. Michaelides, Understanding corrosion inhibition with van der Waals DFT methods: the case of benzotriazole, Faraday Discuss. 180 (2015) 439–458.
[15] J. Walsh, H. Dhariwal, A. Gutierrez-Sosa, P. Finetti, C. Muryn, N. Brookes, R. Oldman, G. Thornton, Probing molecular orientation in corrosion inhibition via a NEXAFS study of benzotriazole and related molecules on Cu (100), Surf. Sci. 415 (1998) 423–432.
[16] C. Gattinoni, P. Tsaousis, C. Euaruksakul, R. Price, D.A. Duncan, T. Pascal, D. Prendergast, G. Held, A. Michaelides, Adsorption behavior of organic molecules: a study of benzotriazole on Cu (111) with spectroscopic and theoretical methods, Langmuir 35 (2019) 882–893.
[17] X. Chen, H. Häkkinen, Divide and protect: passivating Cu (111) by Cu-(benzotriazole) 2, J. Phys. Chem. C 116 (2012) 22346–22349.
[18] K. Cho, J. Kishimoto, T. Hashizume, T. Sakurai, An observation of benzotriazole (BTA) adsorption on Cu (110) by the ultra high vacuum (UHV)-scanning tunneling microscope (STM) and low energy electron difiraction (LEED), Jpn. J. Appl. Phys. 33 (1994) L125.
[19] Y. Park, H. Noh, Y. Kuk, K. Cho, T. Sakurai, Thickness dependent ultraviolet photoemission spectroscopy and scanning tunneling microscopy study of BTA molecular layers on Cu (110), J. Korean Phys. Soc. 29 (1996) 745–749.
[20] K. Cho, J. Kishimoto, T. Hashizume, H. Pickering, T. Sakurai, Adsorption and film growth of BTA on clean and oxygen adsorbed Cu (110) surfaces, Appl. Surf. Sci. 87 (1995) 380–385.
[21] X. Wu, F. Wiame, V. Maurice, P. Marcus, Adsorption and thermal stability of 2-mercaptobenzothiazole corrosion inhibitor on metallic and pre-oxidized Cu (111) model surfaces, Appl. Surf. Sci. 508 (2020), 145132.
[22] X. Wu, F. Wiame, V. Maurice, P. Marcus, 2-Mercaptobenzimidazole films formed at ultra-low pressure on copper: adsorption, thermal stability and corrosion inhibition performance, Appl. Surf. Sci. 527 (2020), 146814.
[23] X. Wu, F. Wiame, V. Maurice, P. Marcus, 2-Mercaptobenzothiazole corrosion inhibitor deposited at ultra-low pressure on model copper surfaces, Corros. Sci. 166 (2020), 108464.
[24] X. Wu, F. Wiame, V. Maurice, P. Marcus, Molecular scale insights into interaction mechanisms between organic inhibitor film and copper, npj Mater. Degrad. 5 (2021) 1–8.

[25] I. Horcas, R. Fernández, J. Gomez-Rodriguez, J. Colchero, J. Gómez-Herrero, A. Baro, WSXM: a software for scanning probe microscopy and a tool for nanotechnology, Rev. Sci. Instrum. 78 (2007), 013705.
[26] CasaXPS software version 2.3.22, Casa Software Ltd, Teignmouth, UK.
[27] G. Kresse, J. Furthmüller, Efficiency of ab-initio total energy calculations for metals and semiconductors using a plane-wave basis set, Comput. Mater. Sci. 6 (1996) 15–50.
[28] G. Kresse, J. Furthmüller, Efficient iterative schemes for ab initio total-energy calculations using a plane-wave basis set, Phys. Rev. B 54 (1996) 11169.
[29] G. Kresse, J. Hafner, Ab initio molecular dynamics for liquid metals, Phys. Rev. B 47 (1993) 558.
[30] J. Klimeš, D.R. Bowler, A. Michaelides, Van der Waals density functionals applied to solids, Phys. Rev. B 83 (2011), 195131.
[31] G. Kresse, D. Joubert, From ultrasoft pseudopotentials to the projector augmented-wave method, Phys. Rev. B 59 (1999) 1758.
[32] N. Simon, E. Drexler, R. Reed, Properties of copper and copper alloys at cryogenic temperatures. Final report, National Institute of Standards and Technology (MSEL), Boulder, CO (United States), 1992.
[33] F. Grillo, D. Batchelor, C.R. Larrea, S.M. Francis, P. Lacovig, N.V. Richardson, On-surface condensation of low-dimensional benzotriazole–copper assemblies, Nanoscale 11 (2019) 13017–13031.
[34] F. Grillo, C. Gattinoni, C.R. Larrea, P. Lacovig, N.V. Richardson, Copper adatoms mediated adsorption of benzotrazole on a gold substrate, Appl. Surf. Sci. 600 (2022), 154087.
[35] F. Grillo, J.G. Torres, M.-J. Treanor, C.R. Larrea, J.P. Goetze, P. Lacovig, H. Früchtl, R. Schaub, N.V. Richardson, Two-dimensional self-assembly of benzotriazole on an inert substrate, Nanoscale 8 (2016) 9167–9177.
[36] K. Salorinne, X. Chen, R.W. Troff, M. Nissinen, H. Häkkinen, One-pot synthesis and characterization of subnanometre-size benzotriazolate protected copper clusters, Nanoscale 4 (2012) 4095–4098.